Cytochrome *c* as a distinct modulator of amyloid-β amyloidogenesis in a peroxide-dependent manner

Zhi Du[1,†], Eunju Nam[1,†], Yuxi Lin[2], Mannkyu Hong[1,3], Tamás Molnár[4], Ikufumi Kondo[5], Koichiro Ishimori[5,6], Mu-Hyun Baik[1,3], Young-Ho Lee[2,7,8,9]*, and Mi Hee Lim[1]*

[1]Department of Chemistry, Korea Advanced Institute of Science and Technology (KAIST), Daejeon 34141, Republic of Korea

[2]Research Center for Bioconvergence Analysis, Korea Basic Science Institute (KBSI), Ochang, Chungbuk 28119, Republic of Korea

[3]Center for Catalytic Hydrocarbon Functionalizations, Institute for Basic Science (IBS), Daejeon 34141, Republic of Korea

[4]Department of Biochemistry, Institute of Biology, Eötvös Loránd University, H-1117 Budapest, Hungary

[5]Graduate School of Chemical Sciences and Engineering, Hokkaido University, Kita 13, Nishi 8, Kita-ku, Sapporo 060-8628, Japan

[6]Chemistry Department, Faculty of Science, Hokkaido University, Kita 10, Nishi 8, Kita-ku, Sapporo 060-0810, Japan

[7]Bio-Analytical Science, University of Science and Technology (UST), Daejeon 34113, Republic of Korea

[8]Graduate School of Analytical Science and Technology (GRAST), Chungnam National University, Daejeon 34134, Republic of Korea

[9]Research Headquarters, Korea Brain Research Institute (KBRI), Daegu 41068, Republic of Korea

[†]These authors contributed equally to this work.

*To whom correspondence should be addressed: miheelim@kaist.ac.kr and mr0505@kbsi.re.kr

Graphical abstract

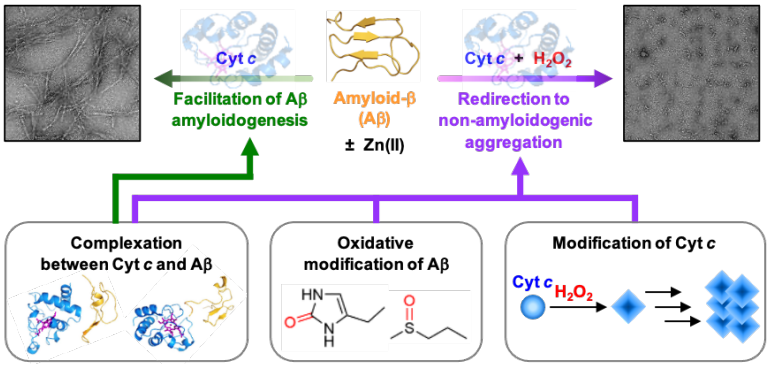

Abstract

Cytochrome *c* (Cyt *c*) is an important, multifunctional protein for controlling cell fate. Emerging evidence suggests a potential role of Cyt *c* in the amyloid pathology associated with Alzheimer's disease (AD); however, the interaction between Cyt *c* and amyloid-β (Aβ) with the consequent impact on the aggregation and toxicity of Aβ is not known. Here we report the discovery that Cyt *c* can directly bind to Aβ and alter the aggregation and toxicity profiles of Aβ in a peroxide-dependent manner. Cyt *c* redirects Aβ peptides into less toxic, off-pathway amorphous aggregates in the presence of hydrogen peroxide (H_2O_2), whereas it accelerates Aβ fibrillization without H_2O_2. Such effects can be achieved by three possible mechanisms, including the complexation between Cyt *c* and Aβ, the oxidation of Aβ by Cyt *c* and H_2O_2, and the H_2O_2-mediated modification of Cyt *c*. Our studies demonstrate a new function of Cyt *c* as a modulator against Aβ amyloidogenesis.

Introduction

As a fatal neurodegenerative disorder, Alzheimer's disease (AD) is characterized by memory loss and cognitive impairment[1-3]. A major pathological hallmark of AD is the deposition of senile plaques primarily composed of amyloid-β (Aβ) aggregates. Aβ self-assembles to generate oligomers, protofibrils, and amyloid fibrils[3-5]. Recent studies suggest that the intertwined networks associated with Aβ and cellular components lead to the complicated pathological nature of AD[3]. Metal ions such as Cu(II) and Zn(II) bind to Aβ peptides, modify their aggregation pathways, and stabilize toxic structured oligomers[5-7]. Furthermore, the overproduction of reactive oxygen species (ROS) triggered by dysregulated redox-active metal ions bound and unbound to Aβ results in oxidative stress with the subsequent impact towards neuronal death[5-9].

As illustrated in Fig. 1a, cytochrome *c* (Cyt *c*) is a globular protein that contains 104 amino acid residues with a covalently attached heme group as a cofactor[10]. In general, Cyt *c* serves as an electron shuttle in the mitochondrial respiratory chain as well as a scavenger against ROS[11]. In addition to mitochondria, Cyt *c* is also found in the cytosol and plays a role in cell differentiation and proliferation[11]. Moreover, extracellular Cyt *c* is reported to promote the survival of hypoxic neurons[12]. Under oxidative stress, Cyt *c* is released from mitochondria to the cytosol[10,13]. When the threshold of Cyt *c* in the cytosol is reached, apoptosis initiates through activating caspases and exhibiting its peroxidase-like activity[11,14]. Aβ is proposed to trigger the efflux of Cyt *c* from mitochondria to the cytosol and, consequently, cause oxidative stress and apoptosis[15,16]. Based on these findings, the reactivities of Cyt *c* with Aβ have been recently explored[17-19]. For example, Cyt *c* significantly attenuated ROS generated by the Aβ–heme complexes *via* direct electron transfer[17]. Studies with Aβ mutants and Cyt *c* exhibited that metal-free Aβ and metal-bound Aβ have distinct electrostatic interactions with Cyt *c*[18]. The mechanism of how Cyt *c* affects the pathology associated with Aβ is not known to date, however.

We questioned whether Cyt *c* directly interacts with Aβ and modifies its aggregation and toxicity profiles. Thus, we evaluated the impact of Cyt *c* on the aggregation of both metal-free Aβ and metal-bound Aβ under normal conditions and oxidative stress as well as the cytotoxicity of the resultant Aβ species. Mechanistic details in the distinct reactivity of Cyt *c* towards Aβ amyloidogenesis in the absence and presence of ROS, including their contacts, conformational changes, and oxidative modifications, were probed. Overall, our work illuminates a novel modulative role of Cyt *c* in the Aβ-related pathology of AD.

Results and discussion

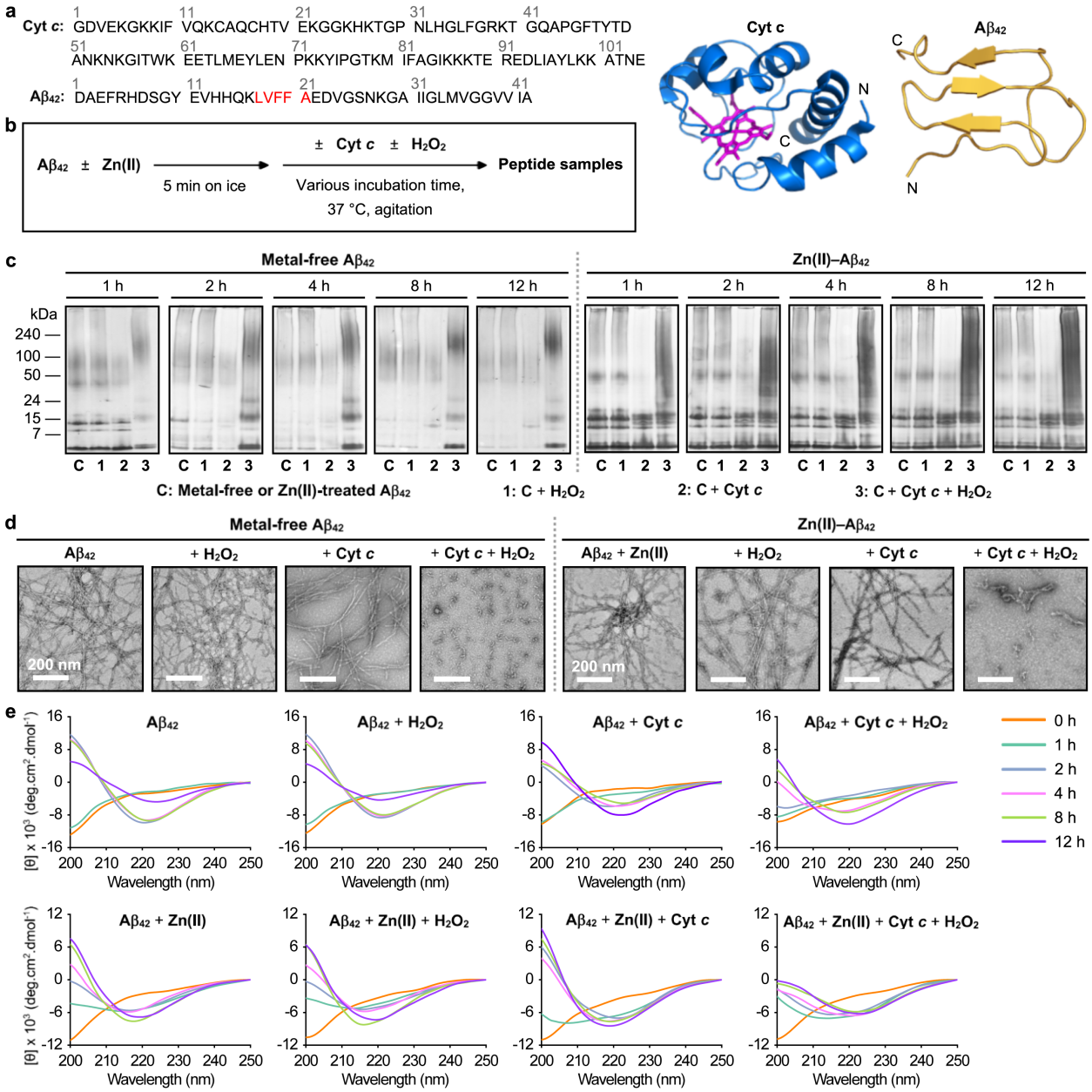

Fig. 1 | Effects of Cyt *c* on the aggregation of metal-free and Zn(II)-bound Aβ42 in the absence and presence of H_2O_2. a, Amino acid sequences and structures of Cyt *c* (PDB 1HRC[23]) and Aβ42 (PDB xx98156[24]). The heme group in Cyt *c* and the self-recognition site of Aβ42 are highlighted in pink and red, respectively. **b,** Scheme of the Aβ42 aggregation experiments with and without Zn(II). **c,** Size distribution of the resultant Aβ42 species at various incubation time points analyzed by gel/Western blot using an anti-Aβ antibody (6E10). **d,** Morphology of the peptide aggregates produced after 12 h incubation visualized by TEM. Scale bars = 200 nm. Conditions: [Aβ42] = 25 μM; [Zn(II)] = 25 μM; [Cyt *c*] = 25 μM; [H_2O_2] = 200 μM; 150 mM HEPES, pH 7.4; 37 °C;

constant agitation (250 rpm). **e,** Change in the secondary structures of metal-free and Zn(II)-treated $A\beta_{42}$ upon aggregation in the presence of Cyt *c* and H_2O_2 observed by CD spectroscopy. $A\beta_{42}$ was incubated with either Cyt *c*, H_2O_2, or both for 0, 1, 2, 4, 8, and 12 h. The spectra of $A\beta_{42}$ with Cyt *c* were obtained by subtracting the features of Cyt *c* under the same conditions. Under the conditions employing 20 mM NaPi buffer, pH 7.4, 150 mM NaF that was chosen to avoid the optical interference from the buffer, the aggregation behavior of $A\beta_{42}$ was similar to that in the HEPES buffer (Supplementary Fig. 1). Conditions: [$A\beta_{42}$] = 40 μM; [Zn(II)] = 40 μM; [Cyt *c*] = 4 μM; [H_2O_2] = 200 μM; 20 mM sodium phosphate (NaPi) buffer, pH 7.4, 150 mM NaF; 37 °C; constant agitation (250 rpm).

Effects of Cyt *c* on the aggregation of metal-free and metal-bound $A\beta_{42}$ with and without ROS. The influence of Cyt *c* on the aggregation of metal-free $A\beta_{42}$ in the absence and presence of H_2O_2 used as a ROS was first monitored by gel electrophoresis with Western blotting (gel/Western blot) using an anti-Aβ antibody (6E10) to determine the molecular weight (MW) distribution of the resultant Aβ species, as described in Fig. 1b and 1c. The band intensities observed in low MWs of $A\beta_{42}$ species in a range of *ca*. 4–15 kDa were weakened upon incubation, indicative of its aggregation. When $A\beta_{42}$ was treated with Cyt *c*, the aggregation of $A\beta_{42}$ was accelerated showing the disappearance of overall bands after 2 h incubation. Distinct from $A\beta_{42}$ with and without Cyt *c*, an increased amount of $A\beta_{42}$ species ranging from 100 to 240 kDa and the bands at low MWs (*ca*. 4–24 kDa) were observed upon treatment of $A\beta_{42}$ with both Cyt *c* and H_2O_2. The size distribution of $A\beta_{42}$ was not significantly changed by H_2O_2 only. Furthermore, the morphology of $A\beta_{42}$ aggregates produced with either Cyt *c*, H_2O_2, or both was visualized by transmission electron microscopy (TEM). As depicted in Fig. 1d, the samples of $A\beta_{42}$ with and without H_2O_2 showed long and thin fibrils after 12 h incubation. When $A\beta_{42}$ was incubated with Cyt *c*, long and thick fibrils were detected. Notably, the addition of both Cyt *c* and H_2O_2 led the generation of amorphous $A\beta_{42}$ aggregates as well as short and flexible protofibrils. Therefore, these results support that Cyt *c* can alter the aggregation of $A\beta_{42}$ in the absence and presence of H_2O_2 to different extents. It should be noted that the impact of Cyt *c* on the aggregation kinetics of $A\beta_{42}$ was not observed by a fluorescent assay because of its signal interference.

To verify the conformational change of $A\beta_{42}$ upon treatment of either Cyt *c*, H_2O_2, or both, the samples were further analyzed by circular dichroism (CD) spectroscopy. We measured the far-UV CD spectra of $A\beta_{42}$ incubated with Cyt *c* in an $A\beta_{42}$-to-Cyt *c* ratio of 10:1 that was selected

to limit Cyt *c*'s signals. At this stoichiometry, Cyt *c* could affect the aggregation of $A\beta_{42}$ (Supplementary Fig. 2). As shown in Fig. 1e, the intensity of the β-sheet of $A\beta_{42}$ species with or without H_2O_2 was deceased by *ca.* 50% over 12 h incubation, indicative of the formation of larger mature fibrils with low solubility. Neither Cyt *c* nor H_2O_2 significantly influenced the change in the secondary structures of $A\beta_{42}$. Different from $A\beta_{42}$ with and without either Cyt *c* or H_2O_2, $A\beta_{42}$ added with both of them formed the β-sheet structure in a slower manner. The overall results obtained by gel/Western blot, TEM, and CD measurements manifest that Cyt *c* can alter the size distribution, morphology, and secondary structures of $A\beta_{42}$ upon aggregation in a peroxide-dependent manner.

As metal ions affect the aggregation of Aβ *via* coordination to Aβ forming metal-bound Aβ (metal–Aβ) complexes[3,5-7], we additionally assessed the impact of Cyt *c* on the aggregation of Zn(II)–$A\beta_{42}$ with and without H_2O_2, as illustrated in Fig. 1b and 1c. It should be noted that we did not probe how Cyt *c* affects the aggregation of Cu(II)–$A\beta_{42}$ in a peroxide-dependent manner because the reaction of Cu(II) with H_2O_2 interferes with our analysis[4]. The sample containing Zn(II)–$A\beta_{42}$ and Cyt *c* indicated a decrease in the amount of $A\beta_{42}$ aggregates (*ca.* 24 to 240 kDa) upon incubation. When Zn(II)–$A\beta_{42}$ was treated with both Cyt *c* and H_2O_2, the smearing in a range of 4–240 kDa was visualized in the gel, which was different from those from the samples of Zn(II)–$A\beta_{42}$ with and without addition of either Cyt *c* or H_2O_2. As shown in Fig. 1d, a mixture of short and flexible protofibrils and amorphous aggregates was detected by incubation of Zn(II)–$A\beta_{42}$ with both Cyt *c* and H_2O_2, compared to long fibrils produced by Zn(II)–$A\beta_{42}$ with and without either Cyt *c* or H_2O_2. As expected, Cyt *c* with H_2O_2 reduced the β-sheet content of Zn(II)–$A\beta_{42}$ species after 2 h incubation, relative to that of Zn(II)–$A\beta_{42}$ only, as summarized in Fig. 1e. These observations confirm the formation of less structured $A\beta_{42}$ aggregates. Collectively, our aggregation investigations corroborate that Cyt *c* can vary the aggregation behaviors of both metal-free $A\beta_{42}$ and Zn(II)-bound $A\beta_{42}$ with and without H_2O_2 to different extents. Particularly, Cyt *c* accelerates the aggregation of $A\beta_{42}$ in the absence of H_2O_2 and redirects Aβ peptides into off-pathway less unstructured assemblies when H_2O_2 is present.

Complexation between Cyt *c* and $A\beta_{42}$. To illuminate how Cyt *c* affects the aggregation of $A\beta_{42}$, the direct interactions between Cyt *c* and $A\beta_{42}$ were first analyzed by electrospray ionization–mass spectrometry (ESI–MS), a soft ionization method for characterizing protein complexes[20]. As depicted in Fig. 2a, new peaks at 1,688 and 1,878 *m/z* corresponding to the complex between Cyt *c* and $A\beta_{42}$ with +10 and +9 charge states, respectively, were detected upon treatment of $A\beta_{42}$

with Cyt *c*. The Cyt *c*–Aβ_{42} adduct in a 1:1 ratio was mainly observed, with the complexes with the Cyt *c*-to-Aβ ratios of 1:2 and 2:1 (Supplementary Fig. 3). The binding of Cyt *c* to Aβ_{42} was further investigated by isothermal titration calorimetry (ITC), as shown in Supplementary Fig. 4. An endothermic ITC isotherm was obtained and the ITC peak intensity decreased as Cyt *c* was titrated into the solution of Aβ_{42}, indicating their intermolecular interactions. The ITC peaks consisted of the two components, the late broad peak following the early sharp peak. The broad ITC peaks may be attributed to the aggregation of Aβ_{42} by Cyt *c*, which would be further boosted because of rigorous stirring in an ITC cell.

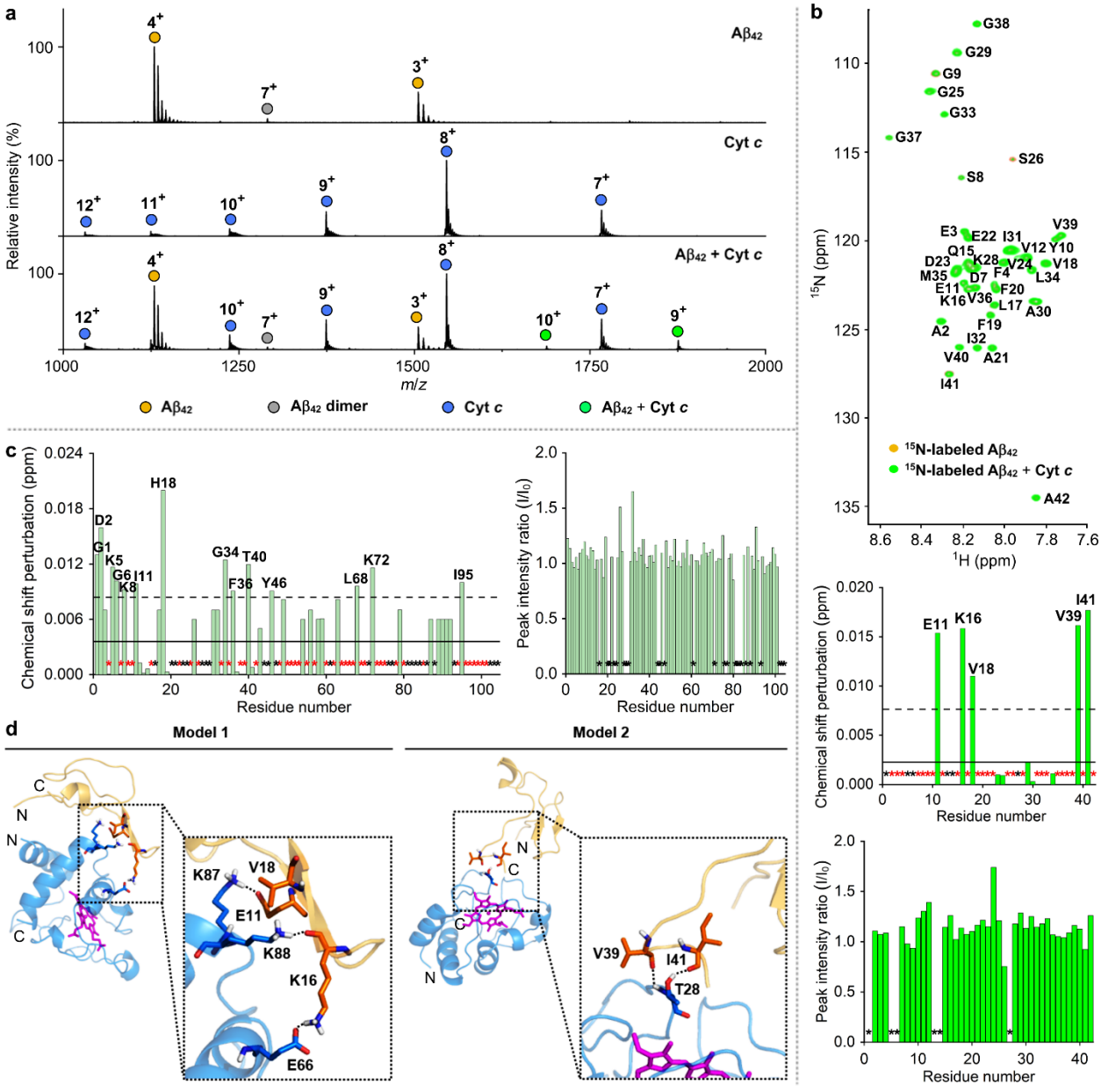

Fig. 2 | Interaction between Cyt *c* and Aβ_{42}. a, Complexation between Cyt *c* and Aβ_{42} detected by ESI–MS. Conditions: [Aβ_{42}] = 100 μM; [Cyt *c*] = 100 μM; 20 mM ammonium acetate, pH 7.4; 37 °C; incubation for 30 min. The samples were diluted by 10-fold prior to injection to the mass spectrometer. **b,** 2D ^{1}H–^{15}N band-selective optimized flip angle short transient–heteronuclear multiple quantum correlation (SOFAST–HMQC) NMR spectra (800 MHz) of ^{15}N-labeled Aβ_{42} monomer with and without Cyt *c*. The average of chemical shift perturbations (CSPs) and the average plus one standard deviation are presented with solid and dashed lines, respectively. Black asterisks represent the amino acid residues that cannot be resolved for analysis, and red asterisks indicate the amino acid residues without detectable CSPs. Conditions: [^{15}N-labeled Aβ_{42}] = 40 μM; [Cyt *c*] = 200 μM; 150 mM HEPES, pH 7.4; 10% v/v D_2O; 10 °C. **c,** Analysis of the CSPs and the change in the peak intensity observed within ^{15}N-labeled Cyt *c* by addition of Aβ_{42}. The 2D ^{1}H–^{15}N heteronuclear single quantum coherence (HSQC) NMR spectra of ^{15}N-labeled Cyt *c* with and without Aβ_{42} monomer are depicted in Supplementary Fig. 5. **d,** Representative models of the Cyt *c*–Aβ_{42} interfaces from the trajectories of MD simulations. Initial conformations of Cyt *c* (PDB 1HRC;[22] blue) and Aβ_{42} (xx98156;[23] yellow) were used for binding studies. The heme group in Cyt *c* is highlighted in pink. Model 1 and 2 of the Cyt *c*–Aβ_{42} adducts are illustrated in Supplementary Fig. 6. Possible hydrogen bonds are depicted with dashed black lines.

Next, the binding properties of Cyt *c* with Aβ_{42} were probed by two-dimensional (2D) nuclear magnetic resonance (NMR) spectroscopy employing either ^{15}N-labeled Aβ_{42} or Cyt *c*. As presented in Fig. 2b, when Cyt *c* was added into uniformly ^{15}N-labeled Aβ_{42}, moderate chemical shift perturbations (CSPs) were detectable near or in the self-recognition and *C*-terminal regions of Aβ_{42} (*e.g.*, Glu11, Lys16, Val18, Val39, and Ile41), respectively, that are critical for Aβ aggregation[2,4]. To further analyze the binding site of Cyt *c* towards Aβ_{42}, we employed ^{15}N-labeled Cyt *c* with 104 amino acid residues that were expressed and purified as previously described[21]. Upon incubation of ^{15}N-labeled Cyt *c* with Aβ_{42}, CSPs were indicated at several amino acid residues of Cyt *c*, including Gly1, Asp2, Lys5, Gly6, Lys8, Ile11, His18, Gly34, Phe36, Thr40, Tyr46, Leu68, Lys72, and Ile95, as displayed in Fig. 2c and Supplementary Fig. 5. This suggests that Aβ_{42} has multiple contacts onto the whole region of Cyt *c*.

To investigate the potential binding modes of Cyt *c* to Aβ_{42}, MD simulations were carried out with an X-ray crystal structure of Cyt *c* (PDB 1HRC[22]) and an Aβ_{42} conformer acquired from the MD simulation data[23], as shown in Fig. 1a. Fig. 2d and Supplementary Fig. 6 describe two

possible Cyt *c*–Aβ_{42} dimeric interfaces associated with two majorly interacting regions (*e.g.*, Glu11, Lys16, and Val18; Val39 and Ile41) of Aβ_{42} shown in 2D NMR studies (Fig. 2b). It should be noted that our MD simulations did not consider the CSPs in Cyt *c* obtained upon addition of Aβ_{42} because they were detected in most of its amino acid residues. The model on the left involves Glu11, Lys16, and Val18 close to the self-recognition site in Aβ_{42} as the major binding region with Cyt *c*. The carboxylate group of Glu11 forms a hydrogen bond with a length of 1.9 Å against the side chain of Lys87 in Cyt *c*. Furthermore, the side chain of Lys16 in Aβ_{42} interacts with Glu66 in Cyt *c* in an average length of 1.9 Å and its backbone carbonyl group exhibits an additional hydrogen bond with Lys88 in Cyt *c*. The hydrophobic Val18 residue of Aβ_{42} resides between two positioned alkyl chains of the aforementioned Lys87 and Lys88 in Cyt *c*. In the other probable model, Thr28 in Cyt *c* plays a key role in interacting with the *C*-terminal region of Aβ_{42} that is anchored to Cyt *c* by the following two hydrogen bonds: (i) the backbone carbonyl group of Val39 in Aβ_{42} and the backbone amide moiety of the Thr28 in Cyt *c*; (ii) the backbone carbonyl group of Ile41 in Aβ_{42} and the side chain hydroxyl group of Thr28 in Cyt *c*. Overall, our ESI–MS, ITC, NMR, and computational studies support that Cyt *c* can interact with Aβ_{42} in a direct but relatively weak binding manner.

Oxidation of Aβ_{42} by Cyt *c* and H_2O_2. Given that ROS cause oxidative modifications of proteins and, consequently, alter their structures and functions[24], we evaluated whether Cyt *c* could oxidize Aβ_{42} in the presence of H_2O_2. Like other heme-containing peroxidases, Cyt *c* with H_2O_2 can catalytically oxidize a wide range of substrates *via* high-valent Fe(IV) intermediates[25]. The peroxidase-like activity of Cyt *c* was measured by the ABTS assay [ATBS = 2,20-azinobis(3-ethylbenzthiazoline-6-sulfonate][26]. Cyt *c* with H_2O_2 noticeably induced the oxidation of ABTS in a concentration- and time-dependent manner while H_2O_2 was not able to significantly oxidize ABTS under our experimental conditions, which suggests its peroxidase-like activity (Supplementary Fig. 7).

Moving forward, we probed the oxidation of Aβ_{42} in the presence of both Cyt *c* and H_2O_2 by ESI–MS. The peaks at 1,133, 1,137, and 1,139 *m*/*z*, assigned to be $[A\beta_{42} + O + 4H]^{4+}$, $[A\beta_{42} + 2O + 4H]^{4+}$, and $[A\beta_{42} + Na + O + 3H]^{4+}$, respectively, were detected, as displayed in Fig. 3a. The peak intensities associated with oxidized $A\beta_{42}{}^{4+}$ species produced by Cyt *c* and H_2O_2 were enhanced, compared to those by H_2O_2 only. To identify the oxidation sites of Aβ_{42} by both Cyt *c* and H_2O_2, tandem MS (ESI–MS^2) with collision-induced dissociation (CID) was performed. A mass shift of 16 Da from y_8 and b_{14}, as presented in Fig. 3b and 3c, indicated that both His14 and Met35 could be oxidized. Oxidized $A\beta_{42}{}^{4+}$ by H_2O_2 at 1,133 *m/z* exhibited Met35 as the oxidation

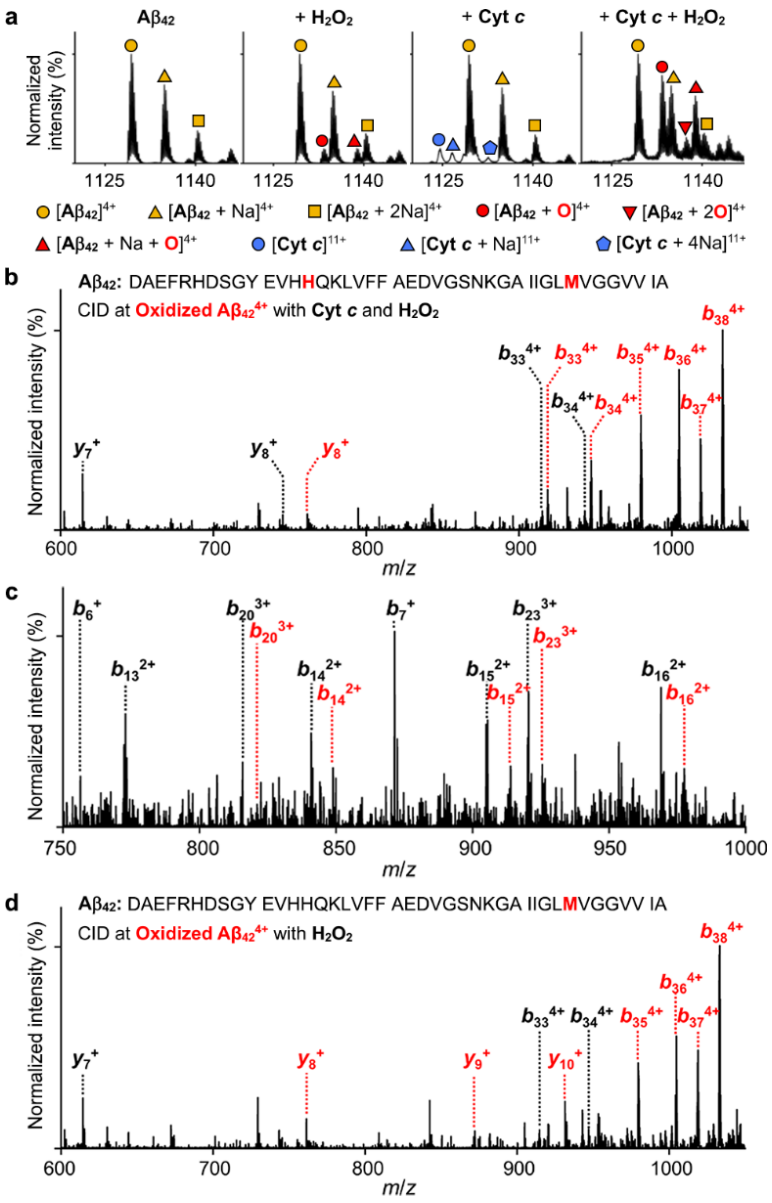

Fig. 3 | Oxidation of Aβ$_{42}$ in the presence of Cyt *c* and H_2O_2 analyzed by ESI–MS and ESI–MS^2. a, ESI–MS spectra of +4-charged Aβ$_{42}$ treated with either Cyt *c*, H_2O_2, or both. Oxidized Aβ$_{42}^{4+}$ obtained upon treatment with both Cyt *c* and H_2O_2 [**b,** 1,133 *m*/*z* (oxidized Aβ$_{42}^{4+}$); **c,** 1,139 *m*/*z* (an adduct of oxidized Aβ$_{42}^{4+}$ with Na^+)] were analyzed by ESI–MS^2. **d,** ESI–MS^2 spectrum of oxidized Aβ$_{42}^{4+}$ produced by H_2O_2. Conditions: [Aβ$_{42}$] = 100 μM; [Cyt *c*] = 100 μM; [H_2O_2] = 1.6 mM; 20 mM ammonium acetate, pH 7.4; 37 °C; incubation for 30 min; without agitation. The 10-fold diluted samples were injected to the mass spectrometer.

site according to a mass shift of 16 Da from b_{35} and y_8, as depicted in Fig. 3d. Moreover, in the case of Zn(II)-added Aβ_{42}, the oxidation sites of Aβ_{42} by both Cyt *c* and H_2O_2 were identical with those illustrated above (Supplementary Fig. 8). These observations regarding Aβ oxidation are consistent with previous reports regarding oxidative modifications onto the Met and His residues in Aβ species isolated from amyloid plaques[27,28]. The Met35 residue in Aβ is highly susceptible to oxidize to sulfoxide or sulfone forms upon exposure to H_2O_2[29,30]. Oxidized Met35 can alter the solubility, aggregation, and cytotoxicity of Aβ *via* decreasing the hydrophobicity of its *C*-terminal region and varying its secondary structures[29-31]. It should be noted that H_2O_2 did not significantly affect Aβ aggregation under our experimental conditions with a concentration of H_2O_2 (200 μM), which was much lower than that used for previous studies (*ca.* 12 mM)[29]. Additionally, the His14 residue participates in Zn(II) binding of Aβ and is oxidized to 2-oxo-histidine[5-7,26,32], which may contribute to the modulative reactivity of Cyt *c* with H_2O_2 against the aggregation of Zn(II)–Aβ. Together, our studies confirm that Cyt *c* significantly triggers oxidative modifications of both metal-free Aβ and Zn(II)–Aβ in the presence of H_2O_2, which consequently affects their aggregation profiles.

Modification of Cyt *c* by H_2O_2. H_2O_2 is reported to induce the oxidative modifications and conformational fluctuations of Cyt *c*, which ultimately enhances its peroxidase-like activity and triggers its aggregation[33-35]. We questioned whether H_2O_2 triggers the aggregation of Cyt *c* under our experimental conditions with the consequent impact on the aggregation of metal-free and Zn(II)-bound Aβ_{42}. Thus, the size distribution, morphology, and change in the secondary structures of the resultant Cyt *c* species upon incubation were analyzed by gel/Western blot, TEM, and CD spectroscopy, as summarized in Fig. 4. In the samples of Cyt *c* with H_2O_2 regardless of the presence of Zn(II), the smearing bands in the gels ranging from *ca*. 35 to 240 kDa were observed within 1 h, indicative of the formation of its aggregates, with the bands at *ca*. 12 and 24 kDa corresponding to monomeric and dimeric Cyt *c*, as illustrated in Fig. 4b. Additionally, small-sized Cyt *c* aggregates were visualized by TEM when Cyt *c* was added with H_2O_2 (Fig. 4c). Moreover, the samples containing Cyt *c* and H_2O_2 with and without Zn(II) exhibited a decrease in the predominant α-helical structure (negative peaks at *ca*. 208 and 222 nm) and an increase in the random coil content (positive peak at *ca*. 214 nm)[25], as monitored by CD spectroscopy (Fig. 4d). It should be noted that the treatment of both metal-free Aβ_{42} and Zn(II)–Aβ_{42} without H_2O_2 did not induce the aggregation of Cyt *c* (Supplementary Fig. 9).

The effect of H_2O_2 on the structural alteration of Cyt *c* was further investigated by 2D ^{1}H–

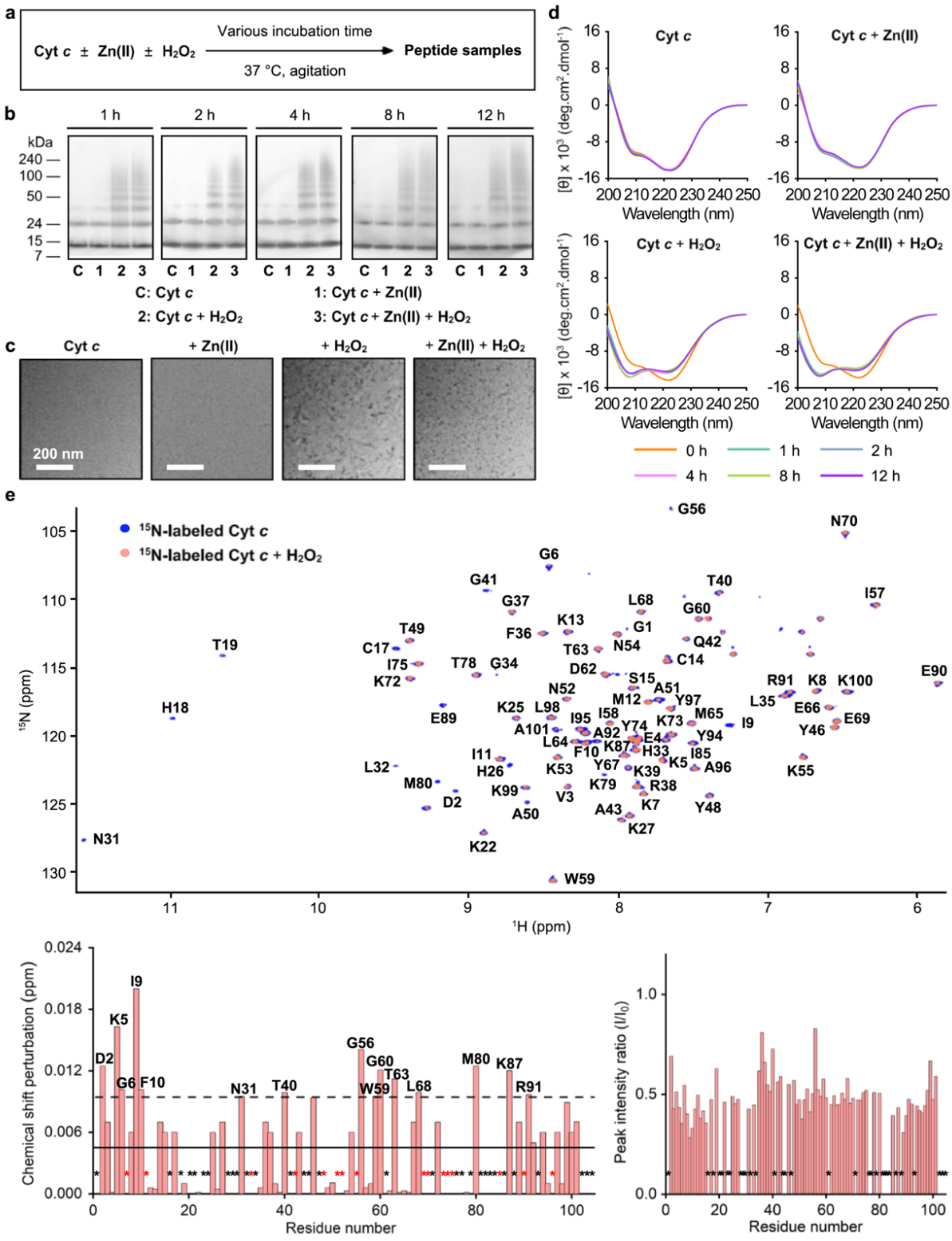

Fig. 4 | Aggregation of Cyt *c* induced by H_2O_2. a, Scheme of the aggregation experiments. **b,** Size distribution of the resultant Cyt *c* species after incubation for 1, 2, 4, 8, and 12 h analyzed by

gel/Western blot using an anti-Cyt *c* antibody. **c,** Morphology of the Cyt *c* aggregates produced over 12 h incubation visualized by TEM. Scale bars = 200 nm. Conditions: [Cyt *c*] = 25 μM; [Zn(II)] = 25 μM; [H_2O_2] = 200 μM; 150 mM HEPES, pH 7.4; 37 °C; constant agitation (250 rpm). **d,** Change in the secondary structures of Cyt *c* upon aggregation in the presence of Zn(II) and H_2O_2 monitored by CD spectroscopy. Cyt *c* was incubated with either Zn(II), H_2O_2, or both for 0, 1, 2, 4, 8, and 12 h. Conditions: [Cyt *c*] = 40 μM; [Zn(II)] = 40 μM; [H_2O_2] = 320 μM; 20 mM NaPi buffer, pH 7.4, 150 mM NaF; 37 °C; constant agitation (250 rpm). **e,** 2D ^{1}H–^{15}N HSQC NMR spectra (800 MHz) of ^{15}N-labeled Cyt *c* with and without H_2O_2. The average of CSPs and the average plus one standard deviation are depicted with solid and dashed lines, respectively. Black asterisks represent the amino acid residues that cannot be resolved for analysis, and red asterisks indicate the amino acid residues without detectable CSPs. Conditions: [^{15}N-labeled Cyt *c*] = 20 μM; [H_2O_2] = 160 μM; 20 mM HEPES, pH 7.4; 10% v/v D_2O; 10 °C.

^{15}N NMR spectroscopy. As presented in Fig. 4e, upon addition of H_2O_2 into ^{15}N-labeled Cyt *c*, moderate CSPs of Asp2, Lys5, Gly6, Ile9, Phe10, Asn31, Thr40, Gly56, Trp59, Gly60, Thr63, Leu68, Met80, Lys87, and Arg91 were observed. Furthermore, H_2O_2 significantly decreased the overall peak intensity of Cyt *c*, which could result from the H_2O_2-mediated generation of NMR-invisible Cyt *c* aggregates. When ^{15}N-labeled Cyt *c* was incubated with both H_2O_2 and $A\beta_{42}$, the Asp2, Ile9, Lys27, Lys39, Thr40, Gly56, and Arg91 residues indicated relatively significant CSPs, compared to those with H_2O_2 only (Supplementary Fig. 10). H_2O_2 and $A\beta_{42}$ greatly enhanced the peak intensity of several amino acid residues, indicating that $A\beta_{42}$ can interact with Cyt *c* aggregates. It should be noted that no substantial difference in the CSP and signal intensity of ^{15}N-labeled $A\beta_{42}$ was observed by treatment of H_2O_2 (Supplementary Fig. 11a), in good agreement with the conclusion drawn from our gel/Western blot, TEM, and CD measurements. Upon treatment of Cyt *c* and H_2O_2, the Asp23 and Gly29 residues of ^{15}N-labeled $A\beta_{42}$ were subject to greater CSPs, as depicted in Supplementary Fig. 11b. The peak intensity was also noticeably reduced, which may be caused by the co-aggregation of $A\beta_{42}$ and Cyt *c*.

To determine whether Cyt *c* aggregates and native Cyt *c* modify the aggregation of $A\beta_{42}$ in a distinct manner, we prepared Cyt *c* aggregates by incubating Cyt *c* with H_2O_2 for 12 h, as illustrated in Supplementary Fig. 12a. After incubation with preformed Cyt *c* aggregates, the change in the band intensity of monomeric $A\beta_{42}$ over time was different from that with or without native Cyt *c* (Supplementary Fig. 12b). In addition, the smearing in a range of 50–240 kDa

indicated the distinct influence of Cyt *c* aggregates on $A\beta_{42}$ aggregation, relative to that of Cyt *c* with and without H_2O_2, which was also confirmed by morphological variations observed from TEM (Supplementary Fig. 12c). These observations manifest that the modification of Cyt *c* triggered by H_2O_2 was another driving force for modifying $A\beta_{42}$ aggregation.

Influence of Cyt *c* and H_2O_2 on the cytotoxicity induced by metal-free $A\beta_{42}$ and Zn(II)–$A\beta_{42}$. To evaluate the cytotoxicity of metal-free and Zn(II)-added $A\beta_{42}$ species produced by the addition of Cyt *c* and H_2O_2, we conducted the MTT assay [MTT: 3-(4,5-dimethylthiazol-2-yl)-2,5-diphenyltetrazolium bromide] employing a human neuroblastoma SH-SY5Y cell line. For the cell viability assay, we prepared metal-free and Zn(II)-treated $A\beta_{42}$ aggregates by 12 h incubation with Cyt *c* in the absence and presence of H_2O_2, and cells were incubated with the resultant aggregates for 24 h, as depicted in Fig. 5. Cyt *c* with and without H_2O_2 generated metal-free $A\beta_{42}$ aggregates that showed less cytotoxicity by approximately 15% and 7%, respectively, than those untreated with either Cyt *c*, H_2O_2, or both. In the case of preformed Zn(II)–$A\beta_{42}$ aggregates, cell viability was improved by about 6% and 20%, respectively, with addition of Cyt *c* in the absence and presence of H_2O_2. These results illustrate that the aggregates of metal-free $A\beta_{42}$ and Zn(II)–$A\beta_{42}$ produced with Cyt *c* have distinct cytotoxicity depending on the presence of H_2O_2, which is supported by the aggregation studies described in Fig. 1. Notably, amorphous metal-free and Zn(II)-treated $A\beta_{42}$ aggregates obtained with both Cyt *c* and H_2O_2 shown in Fig. 1d were less toxic than those with either Cyt *c* or H_2O_2 and without both. It should be noted that the amounts of Cyt *c* and H_2O_2 used for cell studies did not cause cytotoxicity under our experimental conditions (Supplementary Fig. 13). Our cell and aggregation results suggest the regulatory reactivity of Cyt *c* towards the aggregation and toxicity of Aβ particularly in the presence of ROS.

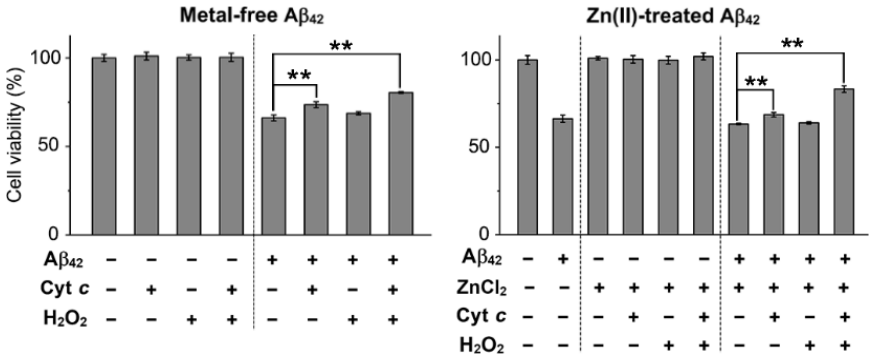

Fig. 5 | Influence of Cyt *c* on the cytotoxicity induced by metal-free and Zn(II)-treated $A\beta_{42}$

species with and without H_2O_2. SH–SY5Y cells were treated with metal-free and Zn(II)-added $A\beta_{42}$ species generated by 12 h treatment with either Cyt *c*, H_2O_2, or both followed by 24 h incubation. Cell viability, determined by the MTT assay, was calculated in comparison to that with an equivalent amount of the buffered solution. Conditions: [$A\beta_{42}$] = 10 μM; [Cyt *c*] = 10 μM; [Zn(II)] = 10 μM; [H_2O_2] = 80 μM; 150 mM HEPES, pH 7.4. Data are represented as mean ± s.e.m. ***P* < 0.01 by Student's test.

Conclusion

As a protein whose localization and function depend on cellular conditions, Cyt *c* plays a critical role in various cellular processes that are involved in respiration, apoptosis, and redox signaling and, thus, is closely related to the development of neurodegenerative diseases such as AD[10,13,36]. Recent findings suggest the reactivity of Cyt *c* with Aβ[17-19]; however, details on whether and how Cyt *c* affects the aggregation and toxicity of Aβ are not known thus far. We report, *for the first time*, the distinct modulative function of Cyt *c* against the amyloidogenesis of both metal-free Aβ and metal-bound Aβ in a peroxide-dependent manner, to the best of our knowledge.

Our multidisciplinary investigations illuminate that Cyt *c* can change the size distribution, morphology, and secondary structures of both metal-free Aβ and Zn(II)–Aβ to different extents. As summarized in Fig. 6, while Aβ amyloidogenesis is accelerated by Cyt c in the absence of H_2O_2, Cyt *c* with H_2O_2 redirects $A\beta_{42}$ peptides into less toxic off-pathway aggregates. These effects are observed regardless of the presence of Zn(II) and may be directed by three possible mechanisms: (i) the complexation between Cyt *c* and Aβ, (ii) the oxidation of Aβ by Cyt *c* and H_2O_2, and (iii) the H_2O_2-mediated modification of Cyt *c*. Our experimental studies with computer simulations support that Cyt *c* directly interacts with the self-recognition and *C*-terminal regions of Aβ that are critical for Aβ aggregation[2,4], in a relatively weak binding manner, which results in facilitating Aβ amyloid formation. Furthermore, Cyt *c* with H_2O_2 promotes oxidative modifications onto the His14 and Met35 residues in Aβ and, thus, alters the its aggregation behavior. Lastly, Cyt *c* aggregates are formed in the presence of H_2O_2, consistent with previously reported studies[25,34], which can notably modify the aggregation of Aβ. Our work demonstrates that Cyt *c* can modulate the aggregation and toxicity profiles of both metal-free and metal-bound Aβ, which validates a new protective role of Cyt *c* in Aβ amyloidogenesis.

Methods

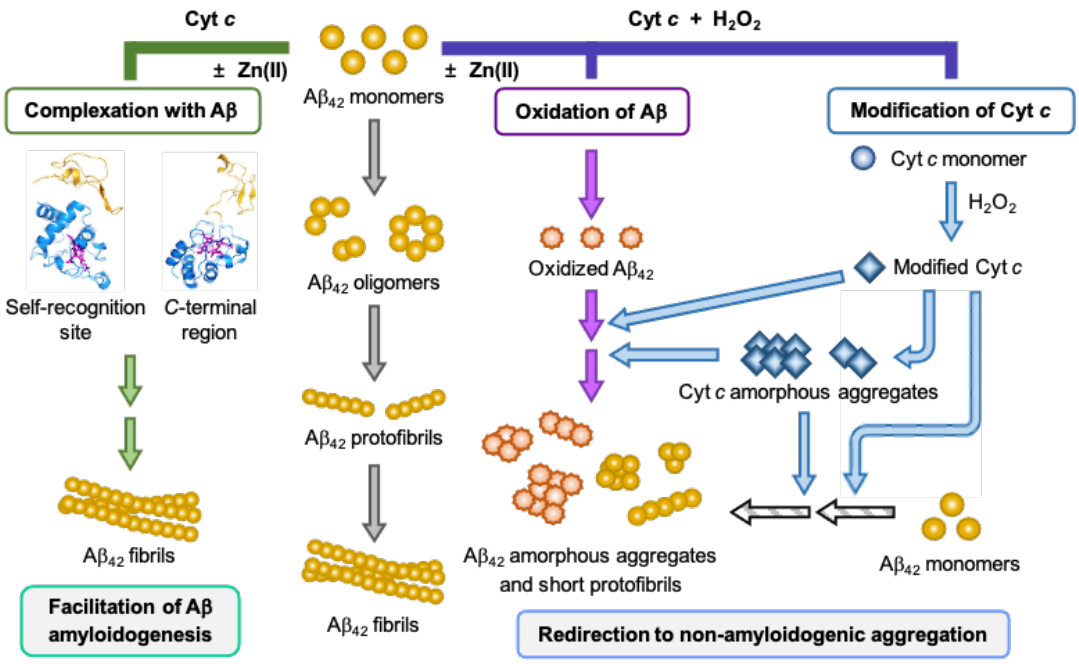

Fig. 6 | Potential mechanisms for the impact of Cyt *c* on Aβ$_{42}$ aggregation in the absence and presence of H_2O_2. Cyt *c* facilitates Aβ$_{42}$ aggregation through their adduct formation in the absence of H_2O_2. Upon incubation of Cyt *c* with Aβ$_{42}$ in the presence of H_2O_2, off-pathway amorphous and less toxic Aβ$_{42}$ aggregates are generated by three possible mechanisms, including (i) the complexation between Cyt *c* and Aβ$_{42}$, (ii) the oxidation of Aβ$_{42}$ by Cyt *c* and H_2O_2, and (iii) the modification of Cyt *c* induced by H_2O_2.

Materials and Methods. All reagents were purchased from commercial suppliers and used as received unless otherwise stated. Aβ$_{42}$ (DAEFRHDSGYEVHHQKLVFFAEDVGSNKGAIIGLMVG-GVVIA) was obtained from Peptide Institute, Inc. (Osaka, Japan) that was purified by high-performance liquid chromatography (HPLC) using YMC Pack ODS-A (YMC CO., LTD., Kyoto, Japan) and Agilent ZORBAX 300SB-C18 columns (Agilent, Santa Clara, CA, USA), respectively. Cyt *c* (from horse heart) was purchased from Sigma-Aldrich (St. Louis, MO, USA). Horse Cyt *c* was employed in the gel/Western blot, CD, TEM, ESI–MS, and ITC measurements as well as cell studies, and ^{15}N-labeled human Cyt *c* was used for 2D ^{1}H–^{15}N NMR experiments. It should be noted that Cyt *c* from mammals exhibits high identity in terms of the amino acid sequences and three-dimensional structures[14]. HEPES [2-(4-(2-hydroxyethyl)piperazin-1-yl)ethanesulfonic acid] was obtained from Sigma-Aldrich. Double-distilled water (ddH_2O) used for all experiments was

obtained from a Milli-Q Direct 16 system (Merck KGaA, Darmstadt, Germany). Trace metal contamination was removed from the solutions used for $A\beta_{42}$ experiments by treating Chelex (Sigma-Aldrich) overnight. The concentrations of proteins were determined by a Shimadzu 1900i UV−visible (UV−Vis) spectrophotometer (Shimadzu, Kyoto, Japan). Experiments by ESI–MS were performed by an Agilent 6530 Accurate Mass Quadrupole Time-of-Flight (Q-TOF) mass spectrometer with an ESI source (Agilent). 2D $^{1}H-^{15}N$ NMR measurements were conducted by a Bruker Avance II 800 NMR spectrometer [Bruker BioSpin, Rheinstetten, Germany; Korea Basic Science Institute (KBSI), Ochang, Republic of Korea] equipped with a cryogenic probe. ITC was performed by a VP-ITC instrument equipped with a motor-driven syringe (Malvern Panalytical, Malvern, UK). The membranes obtained by gel/Western blot were visualized by a ChemiDoc MP Imaging System (Bio-Rad, Hercules, CA, USA). The changes of the secondary structure of proteins were analyzed by a JASCO-815 150-L CD spectropolarimeter [Jasco Inc., Tokyo, Japan; KAIST Analysis Center for Research Advancement (KARA), Daejeon, Republic of Korea]. Morphological changes of protein aggregates were monitored by a Tecnai-G2 Spirit Twin instrument (FEI Company, Eindhoven, Netherlands). MTT [3-(4,5-dimethylthiazol-2-yl)-2,5-diphenyltetrazolium bromide] was purchased from Sigma-Aldrich. Absorbance values for the MTT assay were determined by a SpectraMax M5e microplate reader (Molecular Devices, San Jose, CA, USA).

Acknowledgments

This work was supported by the National Research Foundation of Korea (NRF) grant funded by the Korean government [NRF-2017R1A2B3002585 (M.H.L.); NRF-2019R1A2C1004954 (Y.-H.L.)]; KBSI fund (C220000, C230130, and C230103) (Y.-H.L.); the Institute for Basic Science (IBS-R010-A1) in Korea (M.-H.B.); the Grant-in-Aid for Scientific Research on InnovTive Areas (19H05769) (K.I.). We thank Professor József Kardos (Eötvös Loránd University, Hungary) for providing ^{15}N-labeled recombinant $A\beta_{42}$.

Author contributions

Z.D., Y.-H.L., and M.H.L. designed the research. Z.D. and E.N. performed CD, TEM, ESI–MS, UV–Vis, biochemical assays, and cell studies with data analyses. Y.L. and Y.-H.L. conducted 2D $^{1}H-^{15}N$ NMR and ITC experiments and analyzed the data. M.H. and M.-H.B. carried out MD simulations with analysis. T.M. performed the expression and purification of ^{15}N-labeled recombinant $A\beta_{42}$ and K.I. provided ^{15}N-labeled Cyt *c*. Z.D., E.N., M.H., and M.H.L. wrote the manuscript with input from all authors.

Competing financial interests. The authors declare no competing financial interests.

References

1. Hamley, I. W. The amyloid beta peptide: A chemist's perspective. Role in Alzheimer's and fibrillization. *Chem. Rev.* **112**, 5147-5192 (2012).
2. Kepp, K. P. Bioinorganic chemistry of Alzheimer's disease. *Chem. Rev.* **112**, 5193-5239 (2012).
3. Savelieff, M. G., Nam, G., Kang, J., Lee, H. J., Lee, M. & Lim, M. H. Development of multifunctional molecules as potential therapeutic candidates for Alzheimer's disease, Parkinson's disease, and amyotrophic lateral sclerosis in the last decade. *Chem. Rev.* **119**, 1221-1322 (2019).
4. Lee, S. J., Nam, E., Lee, H. J., Savelieff, M. G. & Lim, M. H. Towards an understanding of amyloid-β oligomers: characterization, toxicity mechanisms, and inhibitors. *Chem. Soc. Rev.* **46**, 310-323 (2017).
5. Han, J., Du, Z. & Lim, M. H. Mechanistic insight into the design of chemical tools to control multiple pathogenic features in Alzheimer's disease. *Acc. Chem. Res.* **54**, 3930-3940 (2021).
6. Atrian-Blasco, E., Gonzalez, P., Santoro, A., Alies, B., Faller, P. & Hureau, C. Cu and Zn coordination to amyloid peptides: From fascinating chemistry to debated pathological relevance. *Coord. Chem. Rev.* **375**, 38-55 (2018).
7. Faller, P., Hureau, C. & Berthoumieu, O. Role of metal ions in the self-assembly of the Alzheimer's amyloid-β peptide. *Inorg. Chem.* **52**, 12193-12206 (2013).
8. Barnham, K. J., Masters, C. L. & Bush, A. I. Neurodegenerative diseases and oxidative stress. *Nat. Rev. Drug Discov.* **3**, 205-214 (2004).
9. Collin, F., Cheignon, C. & Hureau, C. Oxidative stress as a biomarker for Alzheimer's disease. *Biomark. Med.* **12**, 201-203 (2018).
10. Santucci, R., Sinibaldi, F., Cozza, P., Polticelli, F. & Fiorucci, L. Cytochrome *c*: An extreme multifunctional protein with a key role in cell fate. *Int. J. Biol. Macromol.* **136**, 1237-1246 (2019).
11. Garrido, C., Galluzzi, L., Brunet, M., Puig, P. E., Didelot, C. & Kroemer, G. Mechanisms of cytochrome *c* release from mitochondria. *Cell Death Differ.* **13**, 1423-1433 (2006).
12. Liu, H., Sarnaik, S. M., Manole, M. D., Chen, Y., Shinde, S. N., Li, W., Rose, M., Alexander, H., Chen, J., Clark, R. S., Graham, S. H. & Hickey, R. W. Increased cytochrome *c* in rat cerebrospinal fluid after cardiac arrest and its effects on hypoxic neuronal survival.

Resuscitation **83**, 1491-1496 (2012).

13. Alvarez-Paggi, D., Hannibal, L., Castro, M. A., Oviedo-Rouco, S., Demicheli, V., Tortora, V., Tomasina, F., Radi, R. & Murgida, D. H. Multifunctional cytochrome *c*: Learning new tricks from an old dog. *Chem. Rev.* **117**, 13382-13460 (2017).
14. Gonzalez-Arzola, K., Velazquez-Cruz, A., Guerra-Castellano, A., Casado-Combreras, M. A., Perez-Mejias, G., Diaz-Quintana, A., Diaz-Moreno, I. & De la Rosa, M. A. New moonlighting functions of mitochondrial cytochrome *c* in the cytoplasm and nucleus. *FEBS Lett.* **593**, 3101-3119 (2019).
15. Kim, H. S., Lee, J. H., Lee, J. P., Kim, E. M., Chang, K. A., Park, C. H., Jeong, S. J., Wittendorp, M. C., Seo, J. H., Choi, S. H. & Suh, Y. H. Amyloid β peptide induces cytochrome *c* release from isolated mitochondria. *Neuroreport* **13**, 1989-1993 (2002).
16. Morais Cardoso, S., Swerdlow, R. H. & Oliveira, C. R. Induction of cytochrome *c*-mediated apoptosis by amyloid β 25-35 requires functional mitochondria. *Brain Res.* **931**, 117-125 (2002).
17. Ghosh, C., Mukherjee, S. & Dey, S. G. Direct electron transfer between Cyt *c* and heme-Aβ relevant to Alzheimer's disease. *Chem. Commun.* **49**, 5754-5756 (2013).
18. Sarkar, A., Sengupta, K., Chatterjee, S., Seal, M., Faller, P., Dey, S. G. & Dey, A. Metal binding to Aβ peptides inhibits interaction with cytochrome *c*: Insights from abiological constructs. *ACS Omega* **3**, 13994-14003 (2018).
19. Seal, M., Ghosh, C., Basu, O. & Dey, S. G. Cytochrome *c* peroxidase activity of heme bound amyloid β peptides. *J. Biol. Inorg. Chem.* **21**, 683-690 (2016).
20. Heck, A. J. & Van Den Heuvel, R. H. Investigation of intact protein complexes by mass spectrometry. *Mass Spectrom. Rev.* **23**, 368-389 (2004).
21. Sakamoto, K., Kamiya, M., Uchida, T., Kawano, K. & Ishimori, K. Redox-controlled backbone dynamics of human cytochrome *c* revealed by ^{15}N NMR relaxation measurements. *Biochem. Biophys. Res. Commun.* **398**, 231-236 (2010).
22. Bushnell, G. W., Louie, G. V. & Brayer, G. D. High-resolution three-dimensional structure of horse heart cytochrome *c*. *J. Mol. Biol.* **214**, 585-595 (1990).
23. Yang, W., Kim, B. S., Lin, Y., Ito, D., Kim, J. H., Lee, Y.-H. & Yu, W. Exploring ensemble structures of Alzheimer's amyloid β (1-42) monomer using linear regression for the MD simulation and NMR chemical shift. *bioRxiv*, 2021.2008.2023.457317 (2021).
24. Moldogazieva, N. T., Mokhosoev, I. M., Feldman, N. B. & Lutsenko, S. V. ROS and RNS signalling: adaptive redox switches through oxidative/nitrosative protein modifications. *Free Radic. Res.* **52**, 507-543 (2018).

25. Yin, V., Shaw, G. S. & Konermann, L. Cytochrome c as a peroxidase: Activation of the precatalytic native state by H_2O_2-induced covalent modifications. *J. Am. Chem. Soc.* **139**, 15701-15709 (2017).
26. Han, J., Lee, H. J., Kim, K. Y., Nam, G., Chae, J. & Lim, M. H. Mechanistic approaches for chemically modifying the coordination sphere of copper–amyloid-β complexes. *Proc. Natl. Acad. Sci. U. S. A.* **117**, 5160-5167 (2020).
27. Dong, J., Atwood, C. S., Anderson, V. E., Siedlak, S. L., Smith, M. A., Perry, G. & Carey, P. R. Metal binding and oxidation of amyloid-β within isolated senile plaque cores: Raman microscopic evidence. *Biochemistry* **42**, 2768-2773 (2003).
28. Atwood, C. S., Huang, X., Khatri, A., Scarpa, R. C., Kim, Y. S., Moir, R. D., Tanzi, R. E., Roher, A. E. & Bush, A. I. Copper catalyzed oxidation of Alzheimer Abeta. *Cell. Mol. Biol.* **46**, 777-783 (2000).
29. Hou, L., Kang, I., Marchant, R. E. & Zagorski, M. G. Methionine 35 oxidation reduces fibril assembly of the amyloid Aβ(1–42) peptide of Alzheimer's disease. *J. Biol. Chem.* **277**, 40173-40176 (2002).
30. Johansson, A. S., Bergquist, J., Volbracht, C., Paivio, A., Leist, M., Lannfelt, L. & Westlind-Danielsson, A. Attenuated amyloid-β aggregation and neurotoxicity owing to methionine oxidation. *Neuroreport* **18**, 559-563 (2007).
31. Triguero, L., Singh, R. & Prabhakar, R. Comparative molecular dynamics studies of wild-type and oxidized forms of full-length Alzheimer amyloid β-peptides Aβ (1–40) and Aβ (1–42). *J. Phys. Chem. B* **112**, 7123-7131 (2008).
32. Hureau, C. & Faller, P. Aβ-mediated ROS production by Cu ions: structural insights, mechanisms and relevance to Alzheimer's disease. *Biochimie* **91**, 1212-1217 (2009).
33. Tomaskova, N., Novak, P., Kozar, T., Petrencakova, M., Jancura, D., Yassaghi, G., Man, P. & Sedlak, E. Early modification of cytochrome *c* by hydrogen peroxide triggers its fast degradation. *Int. J. Biol. Macromol.* **174**, 413-423 (2021).
34. Nam Hoon, K., Moon Sik, J., Soo Young, C. & Jung Hoon, K. Oxidative modification of cytochrome *c* by hydrogen peroxide. *Mol. Cells* **22**, 220-227 (2006).
35. Hashimoto, M., Takeda, A., Hsu, L. J., Takenouchi, T. & Masliah, E. Role of cytochrome *c* as a stimulator of α-synuclein aggregation in Lewy body disease. *J. Biol. Chem.* **274**, 28849-28852 (1999).
36. Guerra-Castellano, A., Marquez, I., Perez-Mejias, G., Diaz-Quintana, A., De la Rosa, M. A. & Diaz-Moreno, I. Post-Translational modifications of cytochrome *c* in cell life and disease. *Int. J. Mol. Sci.* **21**, 8483-8502 (2020).